Microstructural quantification of rapidly solidified undercooled D2 tool steel

J. Valloton[1,2,*], D.M. Herlach[2], H. Henein[1] and D. Sediako[3]

[1] Department of Chemical and Materials Engineering, University of Alberta, Edmonton, Canada, T6G 1H9

[2] Institut für Materialphysik im Weltraum, Deutsches Zentrum für Luft- und Raumfahrt, Cologne, Germany, 51170

[3] School of Engineering, University of British Columbia, Kelowna, Canada, V1V 1V7. Formerly with Canadian Neutron Beam Centre, Canadian Nuclear Laboratories, Chalk River, Canada, K0J 1J0

[*] Corresponding author: valloton@ualberta.ca

Abstract

Rapid solidification of D2 tool steel is investigated experimentally using Electro-Magnetic Levitation (EML) under terrestrial and reduced gravity conditions and Impulse Atomization (IA), a drop tube type of apparatus. IA produces powders 300 to 1400 µm in size. This allows the investigation of a large range of cooling rate (~100-10,000 K/s) with a single experiment. On the other hand EML allows direct measurements of the thermal history, including primary and eutectic nucleation undercoolings, for samples ~ 6-7 mm in diameter. The final microstructures at room temperature consist of retained supersaturated austenite surrounded by eutectic of austenite and M_7C_3 carbides. Rapid solidification effectively suppresses the formation of ferrite in IA, while a small amount of ferrite is detected in EML samples. High primary phase undercoolings and high cooling rates tend to refine the microstructure, which results in a better dispersion of the eutectic carbides. Evaluation of the cell spacing in EML and IA samples show that the scale of the final microstructure is mainly governed by coarsening. EBSD analysis of IA samples reveal that IA powders polycrystalline, regardless of the solidification conditions. EBSD on EML samples reveal strong differences between the microstructure of droplets solidified on ground and in microgravity conditions. While the former ones are polycrystalline with many different grains, the EML sample solidified in µg shows a strong texture with very few much larger grains having twinning relationships. This indicates that fluid flow has a strong influence on grain refinement in this system.

1. Introduction

D2 tool steels are widely used in industry for dies, punches, forming rolls or blades among others because of their good wear and abrasion properties [1]. This is due to the high volume fraction of carbides that precipitate during the eutectic reaction. However, as can be seen in Figure 1, conventional casting methods result in the formation of coarse carbides. The mechanical properties can be further improved by reducing the size and evenly distributing carbides [2]. This can be achieved by using a rapid solidification technique on D2 tool steel to refine the microstructure.

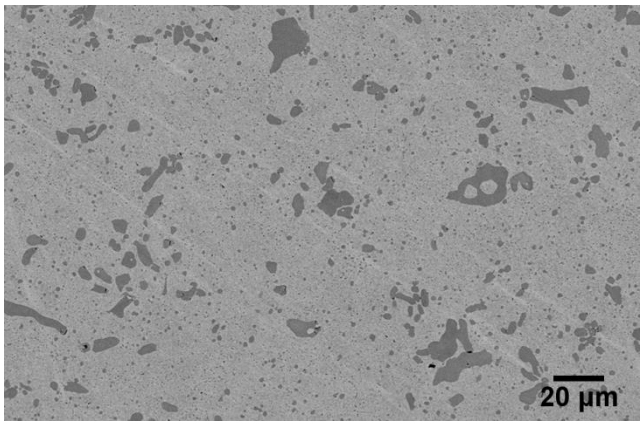

Figure 1: Microstructure of as-received D2 tool steel. The light phase is austenite/ferrite, the dark phase is the M_7C_3 carbide.

Understanding the microstructural evolution during solidification is key to manufacturing products with desired properties. The microstructure evolution during rapid solidification processes depends on the velocity of the solid-liquid interface, which in turn depends on the undercooling ΔT prior to solidification of individual phases in the alloy and the mode of heat extraction. Containerless solidification refers to a class of solidification processes in which large

undercoolings are achieved by the complete avoidance of heterogeneous nucleation on container walls. An undercooled melt corresponds to a non-equilibrium state of metastable liquid. During undercooling, driving forces occur such that in contrast to near-equilibrium solidification there is more than one solidification pathway. The number of possible solidification modes increases with undercooling, making accessible a broad range of metastable microstructures and structurally different phases.

In this study, two containerless techniques, Electro-Magnetic Levitation (EML) and Impulse Atomization (IA), are applied to D2 tool steel. EML enables direct measurement of the primary and eutectic undercoolings for samples ~ 6-7 mm in diameter. IA produces powders 300 to 1400 µm in size. Since the droplet size directly correlates to the cooling rate it allows the investigation of a large range of cooling rate (~100-10,000 K/s) with a single run. Comparisons between results obtained with these two methods allow to investigate the effect of both the undercooling and the cooling rate on the final microstructure of the samples.

2. Experimental methods

D2 tool steel (obtained from Böhler-Uddeholm) is a high carbon, high chromium ferrous alloy with the following composition: Fe-1.55C-11.8Cr-0.4Mn-0.8Mo-0.8V-0.3Si (all in wt.%). A pseudo-binary phase diagram calculated using the ThermoCalc software and TCFE8 database is presented in Figure 2. The dashed line marks the carbon content of D2 tool steel. Under equilibrium conditions, austenite first solidifies at 1667 K (1394°C), followed by the eutectic decomposition of the interdendritic liquid into austenite and carbide ($L \rightarrow \gamma + (Cr,Fe)_7C_3$) at 1543 K (1270°C). At room temperature, the microstructure consists of ferrite and $(Cr,Fe)_7C_3$. However,

during rapid solidification of tool steels metastable supersaturated austenite can be retained in the microstructure [3].

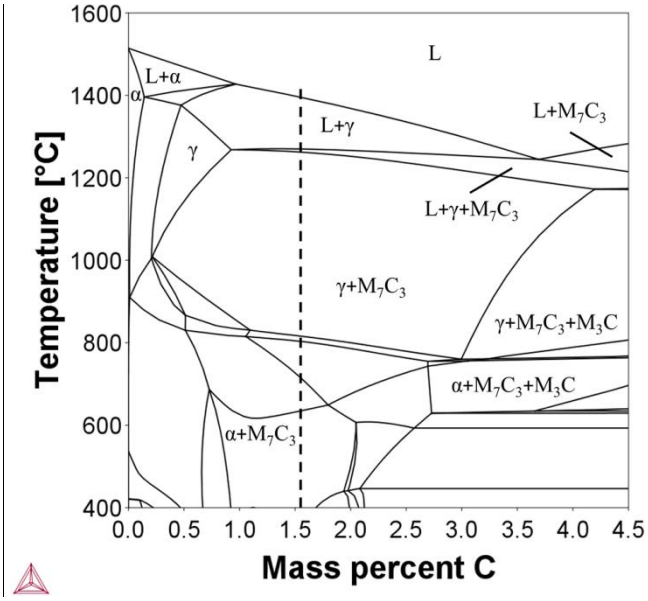

Figure 2: Calculated pseudo-binary phase diagram for D2 tool steel using ThermoCalc software (TCFE8 database). The carbon content of D2 tool steel (1.55 wt.%) is marked by the dashed line. Adapted from [4].

Electro-Magnetic Levitation (EML) is a powerful containerless solidification technique for the processing of electrically conducting samples such as metals and semiconductors with a large range of undercoolings. A schematic view of the apparatus is shown in Figure 3. An alternating current flowing through a water-cooled levitation coil produces an alternating electromagnetic field. A conducting sample placed within this field is levitated by the Lorentz force F_L of the induced eddy currents which compensates for the gravitational force F_G. Simultaneously, the eddy currents induced in the sample heat and melt the sample by ohmic losses. To solidify the sample, cooling jets of inert gas are used. The temperature of the sample is monitored continuously with a two-color pyrometer (Impac IGA10-LO) with an accuracy of ±5 K (a typical

temperature-time profile is shown in Figure 3), while the rapid propagation of the solidification front is observed with a high-speed video camera at 42,000 frames per second (Photron FASTCAM SA5). Detailed information on the EML technique can be found in [5]. EML solidification experiments in reduced gravity conditions were also carried out using the TEMPUS facility (Tiegelfreies ElektroMagentisches Prozessieren Unter Schwerelosigkeit, German for containerless electromagnetic processing in zero-gravity), a portable EML unit specifically designed for parabolic flights [6].

Rods of D2 tool steel were cut into cubes of approximately 5 mm in length (~1 g) and each side was ground to remove any surface paint, oxide layer, and contamination, ensuring that each piece of material was clean. Using an alumina holder, each sample was inserted into the levitation coil in the ultra-high vacuum chamber. The chamber was evacuated to a pressure of 10^{-7} mbar and backfilled with high purity inert gas (helium 6.0). The droplet was melted and overheated to a temperature 100-200 K above its liquidus temperature to remove possible residual oxides and contaminants. To cool the sample below its liquidus temperature and induce solidification, jets of helium 6.0 were then used. The sphere-like sample of 6 to 7 mm in diameter as solidified was retrieved for subsequent characterization.

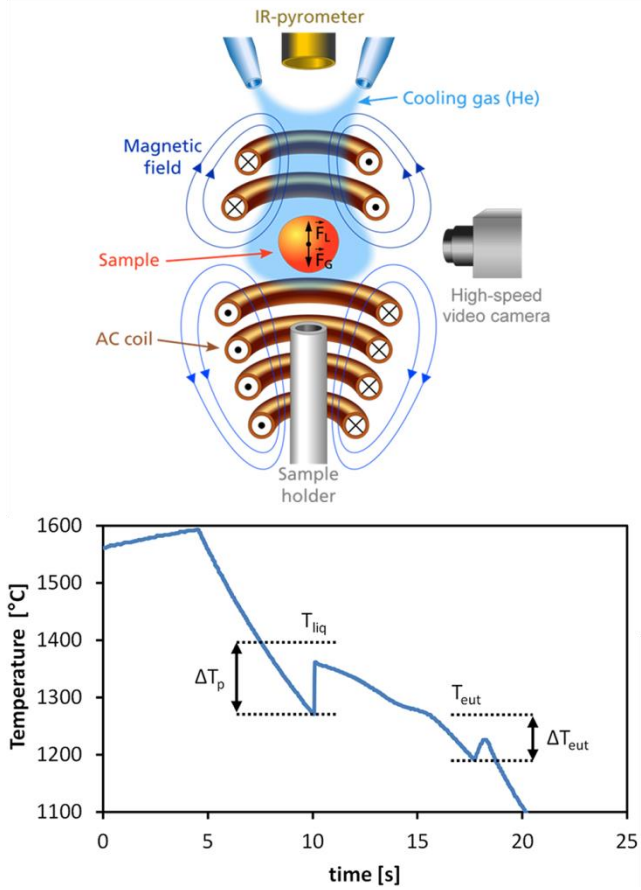

Figure 3: Schematic view of an electromagnetic levitation (EML) apparatus and typical temperature-time profile obtained during EML solidification. Primary and eutectic solidification are clearly identified by the corresponding recalescence events of undercoolings ΔT_p and ΔT_{eut} respectively. Adapted from [4].

Impulse atomization (IA) is the other containerless solidification technique used in this study (Figure 4). It consists in the transformation of a bulk liquid into a spray of liquid droplets. A plunger (or impulse applicator) applies a pressure (or impulse) to the melt in order to push it through a nozzle plate with several orifices of known size and geometry. Liquid ligaments emanate from each orifice, which in turn break up into droplets. Rapid solidification of the droplets then occurs during free fall by heat loss to the surrounding gas (usually He, N_2 or Ar).

Cooling rate is a function of both the droplet size and the gas in the atomization tower. The solidified samples can finally be collected at the bottom of the tower. More information on IA is available in [7].

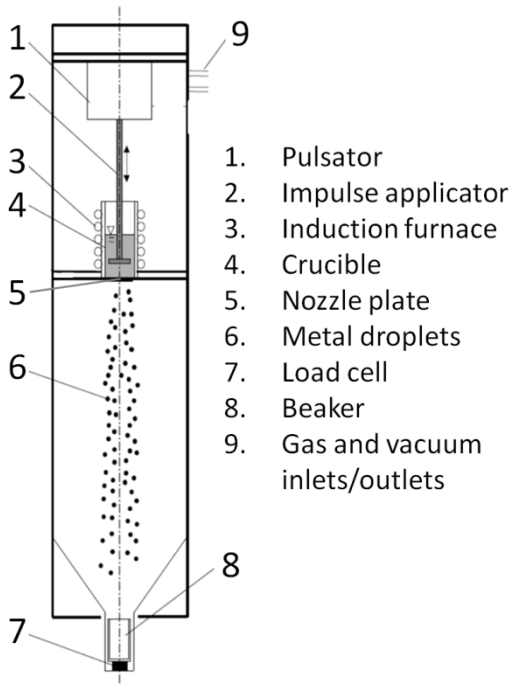

Figure 4: Schematic view of an impulse atomization apparatus.

Rods of D2 tool steel were cut into small pieces and cleaned. The alloy was melted and held in an alumina crucible for 30 min at 1873 K (1600°C, superheat of ~200 K). Then, the liquid was pushed through orifices at the bottom of the crucible to create droplets via atomization. The falling liquid droplets were then cooled in either high purity helium or nitrogen atmospheres having a maximum oxygen content of 8 ppm. The droplets were solidified by the time they reached a high temperature oil quench bath 4 meters below the atomizing nozzle. Subsequently, the IA D2 tool steel powders were washed using toluene and methanol and sieved into different size ranges

based on MPIF Standard [8]. Size ranges of 300-355 µm, 600-710 µm, and 1000-1400 µm were chosen from the IA powders for further characterization.

Contrary to X-Rays, the high penetration of neutrons allows for the analysis of a whole EML sample or an entire population of IA droplets. Neutron diffraction measurements on both EML and IA samples were carried out on the C2 neutron diffractometer of the Canadian Neutron Beam Centre located at the Canadian Nuclear Laboratories in Chalk River, Canada. Measurements were performed using a wavelength of 1.33 Å from a Si531 monochromator at 92.7° 2θ.

In order to reveal the microstructure of the samples, EML and IA samples were mounted in epoxy resin. Grinding was first carried out using silicon carbide papers up to grit 1000 (P2500) , followed by mechanical polishing with 3 and 1 µm diamond particles on soft cloths. Final polishing was performed with a 0.05 µm alumina slurry. The microstructures were then characterized using scanning electron microscopy (SEM) with a Zeiss Sigma FE-SEM running at 20 kV and equipped with an HKL system for Electron Backscattered Diffraction (EBSD).

3. Results and Discussion

Figure 5 shows high-speed video snapshots of electromagnetic levitated samples solidified under different primary undercoolings ΔT_p. The dark grey area is the undercooled liquid. The light grey region corresponds to the growing solid, which appears brighter due to the release of latent heat during recalescence. Tracking of the solid-liquid interface allows for the determination of the growth velocity of the solidification front. At $\Delta T_p \approx 45$ K, a single coarse equiaxed dendrite is growing through the undercooled liquid at a relatively slow velocity, $v \approx 0.03$ m/s (a). At higher undercooling, $\Delta T_p \approx 179$ K, the growth front consists of several fine dendrites originating from a

single nucleation point (b). The growth velocity increases by two orders of magnitude at v ≈ 1.3 m/s. At very high undercooling, ΔT_p ≈ 272 K, the front becomes spherical with no observable dendritic features (c). The growth velocity increases again by almost an order of magnitude to v ≈ 8.4 m/s.

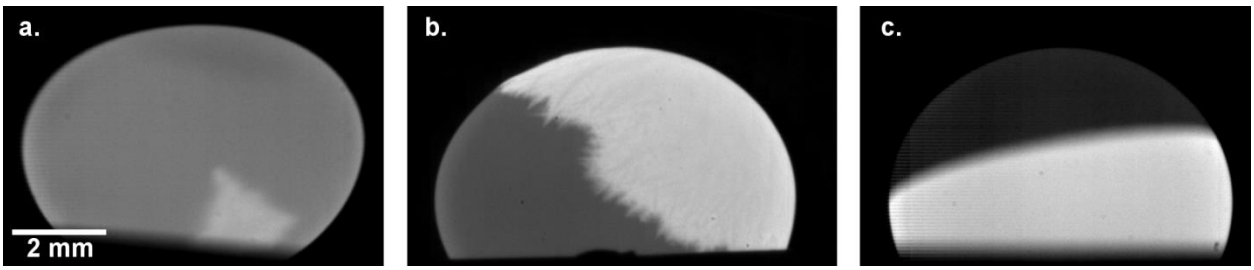

Figure 5: High-speed video images of electromagnetic levitated samples solidified at different primary undercoolings ΔT_p. The dark grey area is the undercooled liquid. The light grey region corresponds to the growing solid, which appears brighter due to the release of latent heat during recalescence. a. ΔT_p ≈ 45 K, v ≈ 0.03 m/s. b. ΔT_p ≈ 179 K, v ≈ 1.3 m/s. c. ΔT_p ≈ 272 K, v ≈ 8.4 m/s. A transition from coarse to fine dendrites to spherical front is observed. Adapted from [4].

Micrographs of the microstructures of these three samples are presented in Figure 6 with both the primary and eutectic undercoolings indicated (ΔT_p and ΔT_e respectively). In all cases, primary austenite and interdendritic austenite + carbide eutectic can be identified. Rapid solidification of D2 seems to suppress completely the formation of ferrite and martensite. However, neutron diffraction experiments performed on 5 different EML samples (1g and µg) with different levels of undercooling yielded small ferrite peaks (see typical spectrum in Figure 7 from the sample shown in Figure 6.c). Rietveld refinement of the spectra showed that a small amount of ferrite is present, about 5-6% in all cases. The level of undercooling does not affect the amount of transformed ferrite. It is thus possible that some ferrite is present in the samples shown in Figure 6, but it could not been identified. At ΔT_p = 45 K a classic coarse grained dendritic microstructure

is observed. Clear dendritic features are found in all samples with a primary undercooling lower than 130 K. At higher undercoolings ($\Delta T_p > 160$ K), these dendritic features disappear in favor of a cellular morphology. This is an indication of spontaneous grain refinement, a rapid solidification phenomenon observed in metals where transitions between coarse columnar and fine equiaxed grain structures are observed at well-defined values of undercooling [9]. However, in the present experiments on D2 tool steel no samples with 130 K < ΔT_p < 160 K were successfully obtained so that the temperature of this transition cannot be accurately determined. It should also be noted that, unlike in other systems [10], no grain refined equiaxed microstructure is observed at smaller undercoolings. High undercoolings give rise to much finer microstructures, with the cell spacing decreasing from 16.8 ± 2.0 µm at ΔT_p = 179 K to 8.3 ± 0.8 µm at ΔT_p = 272 K due to the higher growth velocities involved. This results in a better dispersion of the $(Cr,Fe)_7C_3$ carbides throughout the microstructure. From the high speed video recordings, samples b and c present a very different solidification front morphology. However, the resulting microstructures appear similar with only a difference in their scale. This suggests that the spherical front depicted in Figure 5.c is actually composed of very fine dendrites whose features are too small to distinguish due to the resolution of the camera.

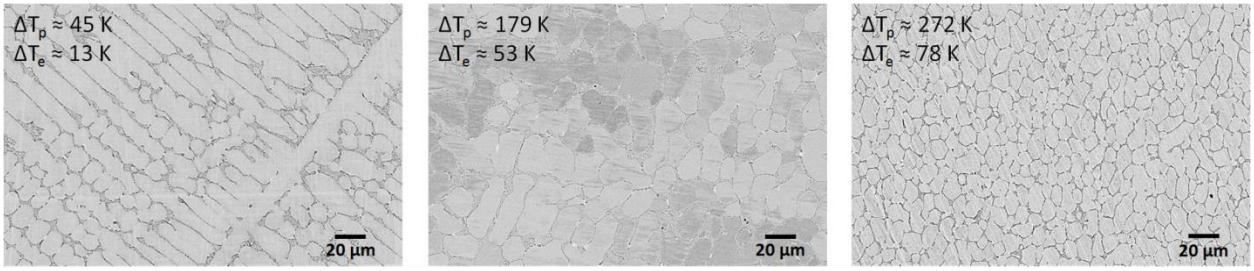

Figure 6: SEM micrographs of cross sections of D2 samples solidified in EML at ΔT_p = 45 K, 179 K, and 272 K respectively. Dendrites or cells of austenite can be observed, surrounded by the eutectic. Adapted from [4].

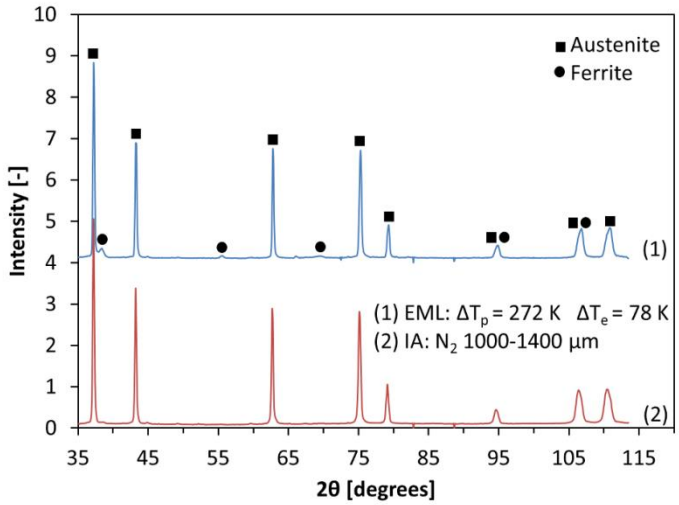

Figure 7: Typical neutron diffraction spectra of EML and IA samples. A small amount of ferrite is detected in the EML sample (~5.2% according to Rietveld refinement).

Eutectic lamellar spacing (λ_{eut}) measurements were performed on high magnification micrographs. The results in Table 1 show that λ_{eut} is the same for EML samples regardless of the undercoolings and processing conditions. However, samples with high eutectic undercoolings see their morphology change from a regular lamellar eutectic to an anomalous globular eutectic in some parts of the samples (Figure 8). A lower attachment-kinetics coefficient is expected for M_7C_3, an ordered compound, than for austenite, a disordered solid solution. The resulting difference in growth velocity at high eutectic undercoolings can suppress the coupled growth conditions. Hence, the leading phase austenite overgrows the more sluggish M_7C_3 and decoupled growth occurs to yield an anomalous eutectic [11][12].

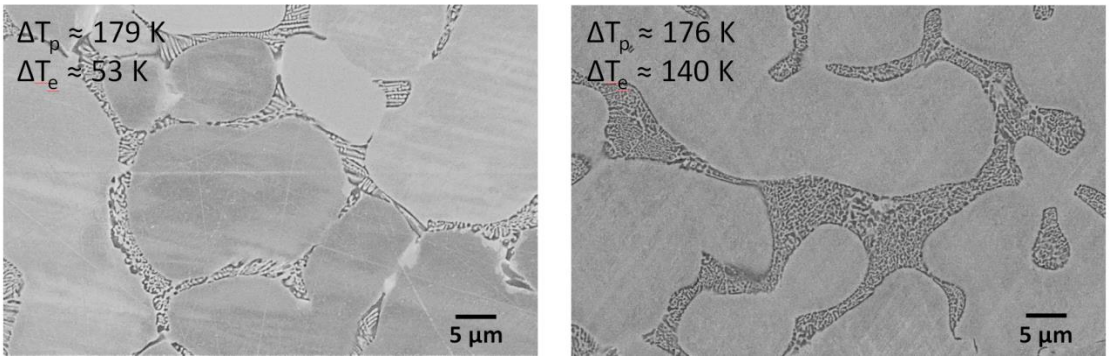

Figure 8: SEM micrographs of cross sections of D2 samples solidified in EML at ΔT_e = 53 K and 140 K respectively. A change from regular lamellar eutectic to anomalous globular eutectic is observed.

Figure 9 shows EBSD maps and the corresponding pole figures for the two high ΔT_p EML samples of Figure 6. Both samples exhibit an equiaxed polycrystalline microstructure. At ΔT_p = 179 K the grain size ranges from 100 to 500 µm while at ΔT_p = 272 K the range decreases to 10 to 50 µm; a stronger grain refinement is observed in the highly undercooled sample. Grain refinement is assumed to be the consequence of fragmentation, i.e. caused by the remelting of the dendrite arms following recalescence [10]. Indeed, looking at the microstructure of the sample solidified at ΔT_p = 45 K in Figure 10, one can again see a dendritic microstructure. However, even at this low primary undercooling there is evidence of fragmentation of the dendrites, with arms seemingly detached from the trunk and surrounded by eutectic. As the undercooling increases, the tip radius decreases, leading to an increase in capillarity effect. Meanwhile, the degree of solute supersaturation increases significantly as the growth velocity of the dendrites increases. Both effects of high undercoolings result in the driving forces for fragmentation becoming large. The refinement of the microstructure observed at high undercoolings is then a consequence of severe fragmentation of the dendrites and subsequent spheroidization of the fragments [13].

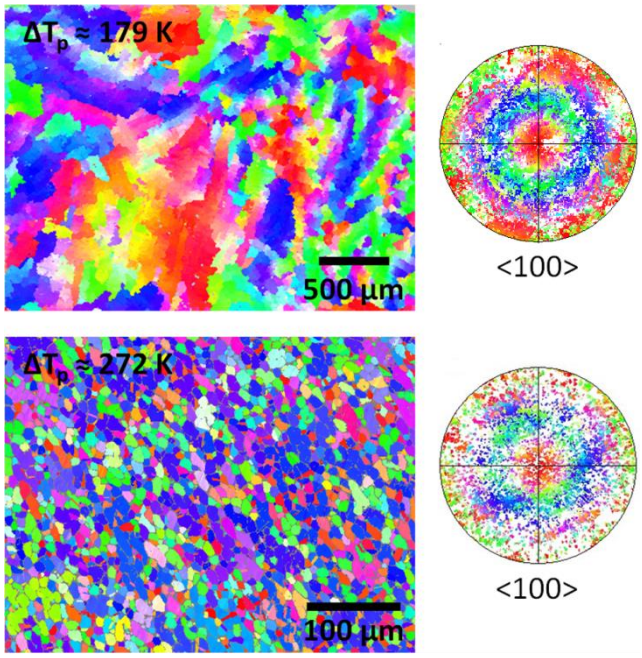

Figure 9: EBSD maps and corresponding pole figures of cross sections of D2 samples solidified in EML at ΔT_p = 179 K (top) and 272 K (bottom). Adapted from [4].

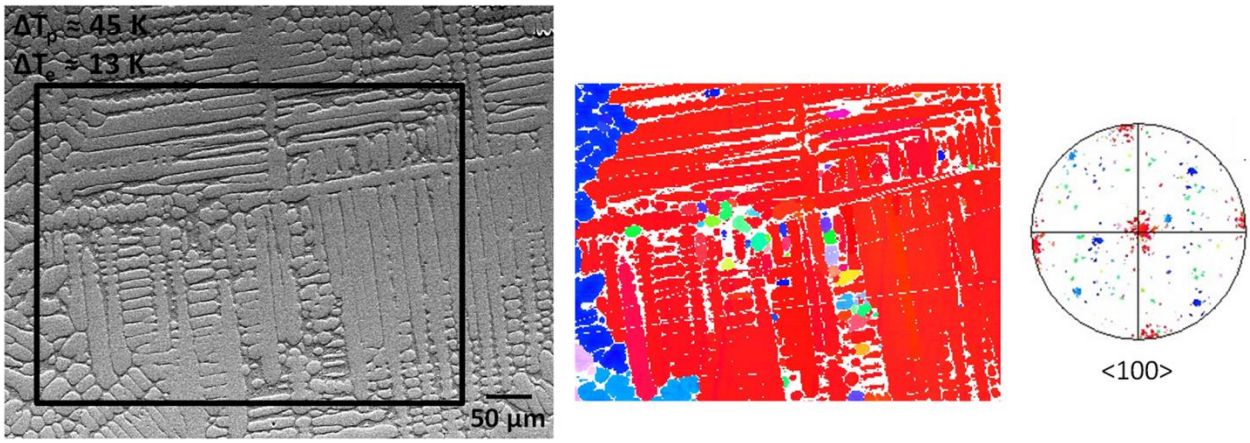

Figure 10: SEM micrograph, EBSD map and corresponding pole figure of a cross section of a D2 samples solidified at ΔT_p = 45 K. Fragmentation of the dendrite arm is observed.

Using the TEMPUS facility in a parabolic flight campaign [6], EML experiments were performed under reduced gravity conditions to observe the influence of convection on the rapid solidification of D2 tool steel. Fluid flow in EML samples processed in microgravity (µg) is reduced

to about 0.05 m/s, compared to 0.3 m/s during ground-based experiments [14]. A typical micrograph of a sample solidified under µg conditions at an undercooling of ΔT_p = 164 K is shown in Figure 11. At first glance the microstructure appears similar to that of the sample solidified on ground at a comparable undercooling (ΔT_p = 179 K in Figure 6), with cells of primary austenite surrounded by the eutectic. Furthermore, the cell size in these two samples is similar (). However, diffraction results are strikingly different. The EBSD map in Figure 12 reveals a strongly textured structure, with only four different grains. Remarkably, these grains have a twin relationship with respect to each other. It is unclear if twinning occurred at nucleation or if solidification started with one single grain with subsequent stacking faults. The size of the largest grain is about 2 mm, potentially more as it is not fully contained within the EBSD map. Such large grains have not been observed in D2 samples solidified at undercoolings of the same magnitude during ground-based experiments. This clearly indicates that fluid flow in the sample during EML solidification plays a major role in grain refinement in this system. This can be explained by considering the grain refinement mechanism described above. From the EBSD map in Figure 10 it can be seen that while most fragments keep the parent orientation of the main <100> dendrite (in red), some fragments do have a different orientation. The latter are mostly found in eutectic-rich region. It is therefore likely that after being completely detached, those fragments were able to rotate freely in the liquid before the eutectic reaction. In microgravity experiments, such fragments would be in a much more quiescent melt. Due to the quasi-absence of fluid flow, the fragments would remain more or less in place and thus keep their original orientation until the eutectic temperature is reached. It is still unclear whether fluid flow also promotes fragmentation of the dendrites via mechanical shear or local remelting due to solute redistribution.

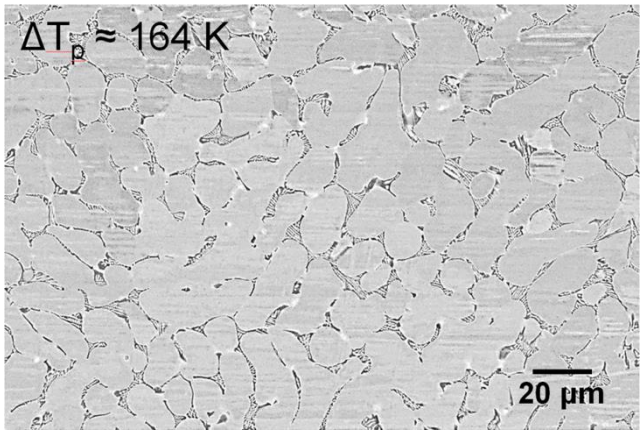

Figure 11: SEM micrograph of a cross section of a D2 sample solidified at ΔT_p = 164 K under reduced gravity conditions.

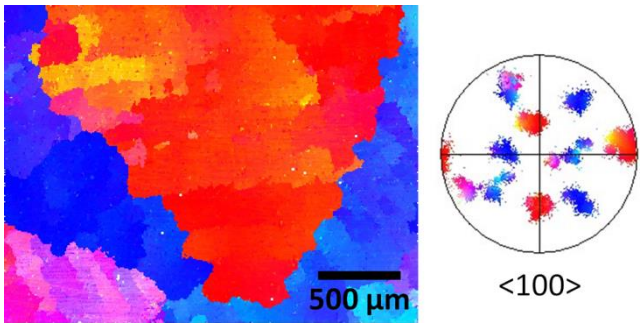

Figure 12: EBSD map and pole figure of a cross section of a D2 sample solidified at ΔT_p = 164 K under reduced gravity conditions.

SEM micrographs of three D2 tool steel droplets produced by IA are shown in Figure 13: a 325 µm particle atomized in helium (left), a 325 µm particle atomized in nitrogen (middle) and a 655 µm particle atomized in nitrogen (right). As in EML samples, austenite and $(Cr,Fe)_7C_3$ carbides can be identified [15]. Furthermore, neutron diffraction indicates that no transformation of austenite to ferrite occurred in 1000-1400 µm droplets solidified in nitrogen (Figure 7). As these experienced the lowest cooling rate of all IA droplets analyzed in this study (~200 K/s for 1000-1400 µm droplets in N_2, an order of magnitude higher than EML experiments), it is expected that formation of ferrite is completely suppressed in IA due to the higher cooling rates compared to

EML. A comparison of the 325 µm particles in Figure 13 shows that the microstructure is finer for particles atomized in helium versus those solidified in nitrogen. The thermal conductivity of helium is significantly higher than that of nitrogen [16]. Thus, droplets atomized in helium solidify faster, resulting in a finer microstructure. Comparing the two particles atomized in nitrogen, it can be seen that the larger particle has a comparatively coarser microstructure. This is because heat transfer, and hence cooling rate, is higher in smaller particles due to their larger surface/volume ratio. It is worth noting that for all IA particles, the average cell spacing is an order of magnitude smaller than what is obtained in EML (Table 1). Hence the dispersion of the $(Cr,Fe)_7C_3$ carbides throughout the microstructure is further improved. The eutectic spacing is also smaller than in the EML samples (Table 1), but is the same order of magnitude. However, higher undercoolings are expected to decrease the lamellar spacing [17]. The small differences observed between the various samples stem from the fact that most of the eutectic likely solidifies after recalescence under quasi-equilibrium conditions. Due to their small sizes, it is more likely to observe the eutectic that formed during recalescence in the IA droplets, thus explaining why the average eutectic spacing is slightly smaller than in EML samples. An in-depth study of the eutectic kinetics in this system will be presented in a subsequent paper.

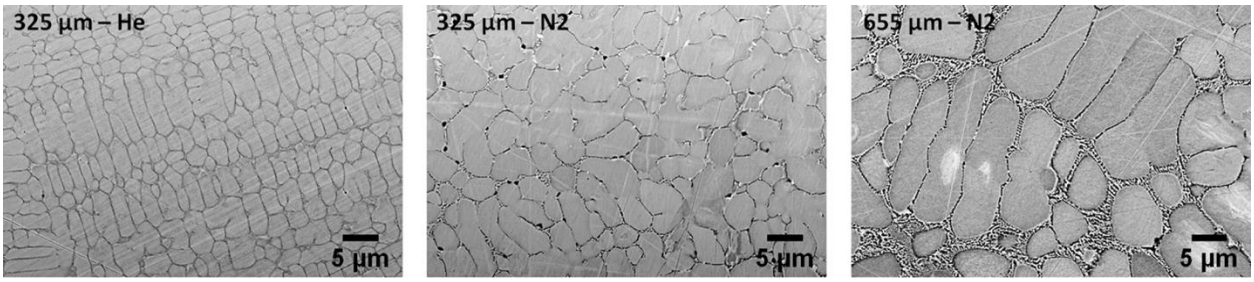

Figure 13: SEM micrographs of cross sections of three D2 particles solidified in IA under different conditions. The microstructure is finer than in EML solidification.

As solidification of IA droplets occurs during free fall, microstructures similar to what is observed in the EML sample solidified in microgravity were expected. However, EBSD analyses reveal that D2 droplets present equiaxed polycrystalline microstructures similar to ground-based EML experiments, regardless of the experimental conditions (Figure 14). As the free-falling droplets are almost devoid of convection, it is unlikely that the various crystallographic orientations found in the microstructure result from fragmentation and coarsening of dendrite arms. Furthermore, previous studies of Al-Fe and Al-Cu samples have shown that IA droplets are usually monocrystalline or have a strong texture [18][19]. It is believed that these polycrystalline structures stem front multiple nucleation events in the undercooled liquid, as observed in Al-Ni droplets [20]. The absence of columnar dendrites at the surface supports nucleation events through the bulk of the samples but the reason for multiple nucleation remains unclear. Droplets solidified in helium (Figure 14 top) exhibit larger and fewer grains than droplets solidified in nitrogen (Figure 14 bottom). As mentioned above, droplets atomized in helium experience higher cooling rates than in nitrogen due to the difference in gas thermal conductivities. The nucleation density being inversely proportional to the cooling rate, droplets solidified in N_2 would then see a higher number of stable clusters, leading to the formation of numerous small grains throughout their volume.

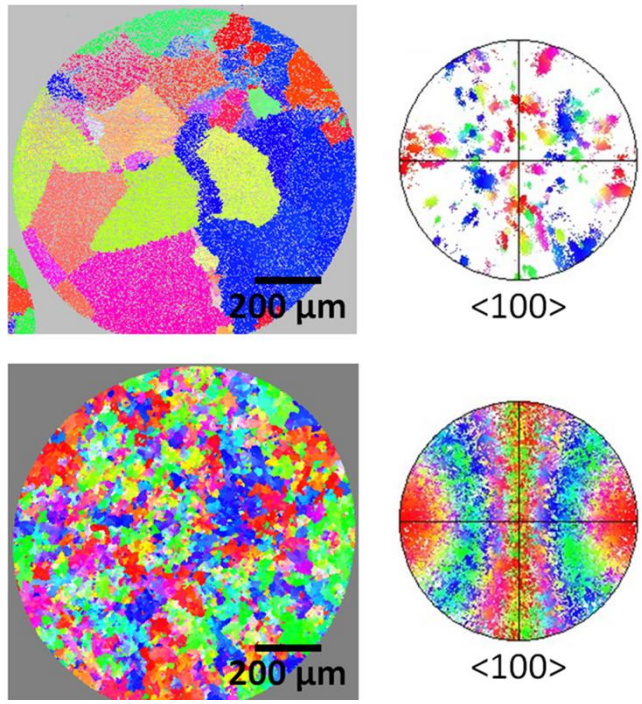

Figure 14: EBSD maps and corresponding pole figures of a 1000-1400 µm IA droplet solidified in He (top) and a 1000-1400 µm droplet solidified in N_2 (bottom).

It is well known that the secondary dendrite arm spacing λ_2 also reveals the solidification cooling rate to a certain extent. λ_2 is shown to be related to the average cooling rate $\dot{T}$ by a power law $\lambda_2 = A\,(\dot{T})^{-n}$ [21]. In order to compare samples solidified in EML and in IA, the secondary dendrite arm spacing (or cell spacing) λ_2 is plotted as a function of the cooling rate in Figure 15. A reasonable fit is obtained with A = 27.9 and n = 0.276. The exponential factor is close to the theoretical value of 1/3 but is lower than the *n* values reported for various steels. However, no such data concerning D2 tool steel could be found [21][22][23]. The observed decrease of λ_2 with cooling rate indicates that the final microstructure of the rapidly solidified samples is controlled in part by coarsening. However, a scatter in the EML data is evident. This is likely due to grain refinement which alters the original microstructure. λ_2 has been measured on dendrites or

dendritic remnant when present. However, as mentioned above, highly undercooled EML samples do not exhibit any dendritic features so that only a cell spacing could be measured. This shows that the effects of undercooling on the final microstructure become important at lower cooling rates.

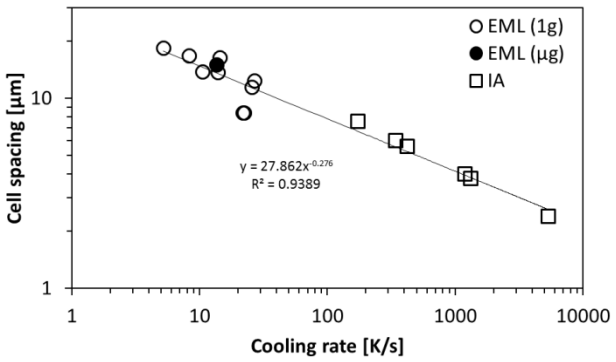

Figure 15: Cell spacing as a function of cooling rate for EML and IA samples.

4. Conclusion

A microstructural study of rapidly solidified D2 tool steel, an industrial alloy, was carried out. Droplets of D2 were solidified over a wide range of undercoolings using Electro-Magnetic levitation and over a wide range of cooling rates using Impulse Atomization. The resulting microstructures consist of dendrites or cells of retained supersaturated austenite surrounded by eutectic of austenite and M_7C_3 carbides. Neutron diffraction confirms the absence of ferrite in IA powders while a small amount is present in EML samples due to the smaller cooling rates involved. EML samples solidified at high primary undercoolings exhibit a fine microstructure with strong grain refinement. Evidence of dendrite fragmentation at low undercooling supports a grain refinement mechanism at high undercoolings consisting of severe fragmentation of the

dendrites and subsequent spheroidization of the fragments. IA results show that higher cooling rates also yield smaller cell spacing and thinner eutectic lamellar spacing. High primary phase undercoolings and high cooling rates tend to refine the microstructure, which results in a better dispersion of the eutectic carbides. EBSD analysis reveals striking differences in microstructures between EML samples solidified on ground and under reduced gravity conditions. Ground-processed samples are found to be polycrystalline with many different grains, while the EML droplet solidified in microgravity exhibits a strong texture, with only a few much larger grains. This indicates that grain refinement in this system is strongly influenced by fluid flow. A steady decrease of cell spacing with increasing cooling rate is observed in IA powders. This shows that the final microstructure is controlled mostly by coarsening. The same trend is observed in EML samples but with more scatter, due to grain refinement which alters the original microstructure at high undercoolings.

Acknowledgment

The authors are grateful to the TEMPUS crew performing the experiment during parabolic flights. The authors also gratefully acknowledge the neutron beamtime and expert support provided by the Canadian Nuclear Laboratories. Dr. M. Kolbe, Dr. T. Volkmann, Dr. J. Gegner, and Dr. C. Karrasch are acknowledged for support and fruitful discussions. Financial support from the Natural Sciences and Engineering Research Council of Canada, the Canadian Space Agency FAST program, and the European Space Agency within the CCEMLCC project under contract #4200020277 is acknowledged.

References

[1] G. Roberts, G. Krauss and R. Kennedy: *Tool Steels*, 5th ed., ASM International, Materials Park, OH, 1998.

[2] Y. Luan, N. Song, Y. Bai, X. Kang, D. Li: *J. Mater. Process. Technolog.*, 2010, vol. 210, pp. 536-541.

[3] A. K. Bhargava and A. N. Tiwari: *Int. J. Rapid Solidification*, 1992, vol. 7, pp. 51-66.

[4] J. Valloton, D. M. Herlach, H. Henein: *IOP Conf. Ser. Mat. Sci.*, 2016, vol. 117, art. no. 012058.

[5] D. M. Herlach and D. M. Matson: *Solidification of Containerless Undercooled Melts*, Wiley-VCH, Weinheim, 1st ed, 2012, pp. 9-16.

[6] G. Lohöfer and J. Piller, *Proc. 40th AIAA Aerospace Sciences Meeting & Exhibit*, 2002, paper no.: AIAA 2002–0764.

[7] H. Henein: *Mater. Sci. Eng.* ,2002, vol. A326, pp. 92-100.

[8] Metal Powder Industries Federation, *Standard test methods for metal powders and powder metallurgy products*, Metal Powder Industry, Princeton, NJ, 2012.

[9] M. Schwarz, A. Karma, K. Eckler and D. M. Herlach: *Phys. Rev. Let.*, 1994, vol. 73, pp. 1380-83.

[10] D. M. Herlach, K. Eckler, A. Karma and M. Schwarz: *Mater. Sci. Eng A*, 2001, vol. 304-306, pp. 20-25.

[11] B. Wei and D. M. Herlach: *Mater. Sci. Eng. A*, 1994, vol. 181-182, pp. 1150-1155.

[12] M. Li and K. Kuribayashi: *Metall. Mater. Trans. A*, 2003, vol. 34, pp. 2999-3008.

[13] M. Behúlová, J. Mesárošová and P. Grgač*: J. Alloys Compd.*, 2014, vol. 615, pp. S217-S223.

[14] J. Lee, D. M. Matson, S. Binder, M. Kolbe, D. M. Herlach and R. W. Hyers: *Metall. Mater. Trans. B*, 2014, vol. 4, pp. 1018-1023.

[15] P. D. Khatibi, A.B. Phillion and H. Henein: *Powder Metall.*, 2014, vol. 57, pp. 70-78.

[16] W. M. Rohsenow and J. P. Hartnett: *Handbook of heat transfer*, 3rd ed., McGraw-Hill, New York, NY, 1998.

[17] J. A. Dantzing and M. Rappaz: *Solidification*, EPFL Press, Lausanne, 1st ed, 2009.

[18] M. Bedel, G. Reinhart, A.-A. Bogno, Ch.-A. Gandin, S. Jacomet, E. Boller, H. Nguyen-Thi and H. Henein: Acta Mater., 2015, vol. 89, pp. 234-246.

[19] J. Valloton, A.-A. Bogno, J. Chen, R. Lengsdorf, H. Henein, D. M. Herlach, U. Dahlborg and M. Calvo-Dahlborg: *TMS 2016: 145 Annual Meeting & Exhibition: Supplemental Proceedings (ed TMS),* John Wiley & Sons, Inc., Hoboken, NJ, pp. 51-57.

[20] A. Ilbagi and H. Henein: *Metall. Mater. Trans. A*, 2014, vol. 45, pp. 2152-2160.

[21] W. Kurz and D. J. Fisher: *Fundamentals of solidification*, 4th ed., Trans Tech Publications, Aedermannsdorf, 1984.

[22] M. Boccalini and H. Goldenstein: *Int. Mat. Rev.*, 2001, vol. 46, pp. 92-115.

[23] O. Volkova, H.-P. Heller and D. Jank: *ISIJ International*, 2003, vol. 43, pp. 1724-1732.

Table 1: Cell spacing (λ_{cell}) and eutectic spacing (λ_{eut}) as function of solidification conditions.

EML	ΔT_{prim} [K]	ΔT_{eut} [K]	λ_{cell} [µm]	λ_{eut} [µm]
	45	13	19.5 ± 1.9	0.37 ± 0.07
	179	53	16.8 ± 2.0	0.38 ± 0.08
	176	140	16.4 ± 1.8	0.38 ± 0.07
	272	78	8.3 ± 0.8	0.37 ± 0.06
µg	164	13	17.3 ± 1.7	0.41 ± 0.09
IA	Gas	Size range [µm]	λ_{cell} [µm]	λ_{eut} [µm]
	He	300-355	2.4 ± 0.3	0.17 ± 0.04
		600-710	4.0 ± 0.7	-
		1000-1400	5.6 ± 1.0	0.23 ± 0.03
	N_2	300-355	3.8 ± 0.1	0.26 ± 0.04
		600-710	6.0 ± 1.1	-
		1000-1400	7.6 ± 1.0	0.21 ± 0.05